A Grid-based Filter for Tracking Bats Applying Field Strength Measurements

Markus Hartmann, Thorsten Nowak, Oliver Pfandenhauer, Jörn Thielecke, Albert Heuberger
Friedrich-Alexander-Universität Erlangen-Nürnberg (FAU), Information Technologies,
91058 Erlangen, Germany
Email: markus.hartmann@fau.de

***Abstract*—Nowadays, many applications demand precise localization information. One of those applications is wildlife monitoring, e.g. tracking of bats. Wireless sensor networks featuring field strength measurements are a promising approach to track tiny and lightweight animals. In this paper a robust grid-based filter for the localization of bats based on field strength measurements is proposed. Therefore, fundamentals of field strength-based direction finding and optimal filtering are presented. A grid-based filtering approach to the problem of field strength-based position estimation of bats is derived and evaluated by Monte Carlo simulations.**

I. Introduction

Wildlife monitoring has become a popular research field, especially in wireless sensor networks (WSNs) [1], [2]. Habitat selection [3] and foraging behavior [4] have been in the focus of research in the past years. With the rapid advance in real-time locating systems (RTLSs) biologists now grasp for the next level of wildlife monitoring, i.e. observing social and behavioral structures of animals. They are interested in interactions and social organization between multiple individuals or inside larger groups.

In the BATS[1] project [**?**] biologists try to understand social interactions between individuals and recognize behavior pattern[5]. In order to answer their research questions a automated localization system is needed that is capable to track multiple bats simultaneously with a observation rate of 1 Hz. Different approaches are already known, e.g. GPS trackers [6] or classical wildlife tracking with cross bearing and VHF-transmitters [7]. All systems have different advantages and disadvantages due to coverage, transmitter weight or update rate. For studying the hunting behavior and social interaction a mid range coverage of approximately $500\,\mathrm{m}$ by $500\,\mathrm{m}$ is desirable.

For accurate tracking of bats in [**?**] a real-time locating system (RTLS) based on time-of-arrival measurements is presented and assessed in terms of its theoretical performance limits. In [8] a system for encounter detection for bats is shown. In [9] and [10] a field strength-based approach is presented which is very cost-effective and is suitable for a mid-range area coverage. In Figure 1 the principal of a RTLS using direction of arrival (DOA) estimation based on received signal strength indication (RSSI) is shown.

[1]Dynamically adaptive applications for bat localization using embedded communicating sensor systems, http://www.for-bats.org/

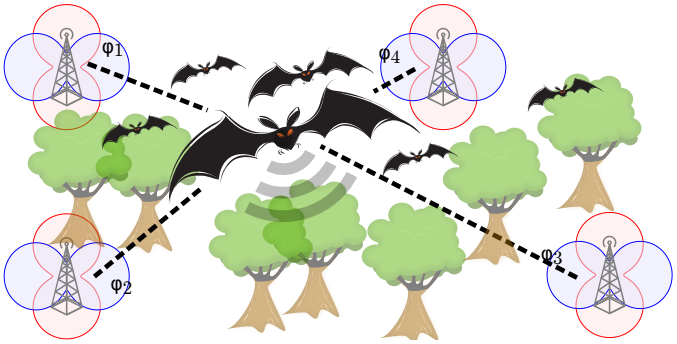

Figure 1: Estimating trajectories of bats: The localization is based on direction finding, which itself is inferred by field strength measurements of radio signals (dashed lines) at two directed antennas (gain patterns denoted in red and blue) at multiple receiver stations. Triangulation of multiple DOA measurements yields the bats position.

A straight-forward approach to track targets based on noisy measurements is Bayesian filtering, the most popular in this domain being the Kalman Filter. However, Kalman Filters and its derivatives (e.g. Extended Kalman Filter) are not able to cope with highly nonlinear models and multimodal distributions. Due to this fact, sub-optimal filtering methods have to be considered in the presented scenario, with particle filters and grid-based filter being the most prominent ones [11]. Particle filter commonly suffer from particle depletion and the "kidnapped robot problem" [12], where the only vital hypothesis might be trapped. Furthermore, the presence of a bat in the observation area is rather short in terms of time and only a small number of measurements are available, so that the particle filter will be frequently re-initialized with uniformly spreading particles over the state space. Therefore, for the localization in the BATS scenario a grid-based filter [13] is implemented and discussed in detail in this paper.

This paper is organized as follows. Section II gives an introduction to the fundamentals of field strength-based DOA estimation and introduces the system model. In Section III the basics of Bayesian filtering are wrapped up and the grid-based filter is introduced. Section IV covers the simulation environment and the filter realization, and in Section V simulation results applying the proposed filter are discussed. Section VI concludes the paper.

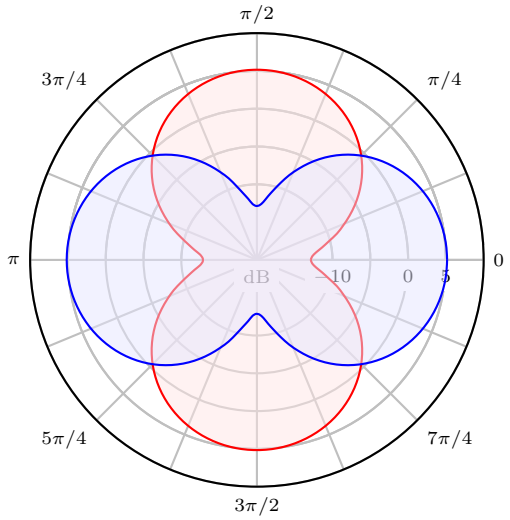

Figure 2: Far-field antenna gain patterns $G_{RX,1}(\varphi)$ (blue) and $G_{RX,2}(\varphi)$ (red) for a antennas provided by a dipole array with a radius of $r = 0.23\lambda$ and at a rotation angle of $\nu = \frac{1}{2}$ between the two antennas.

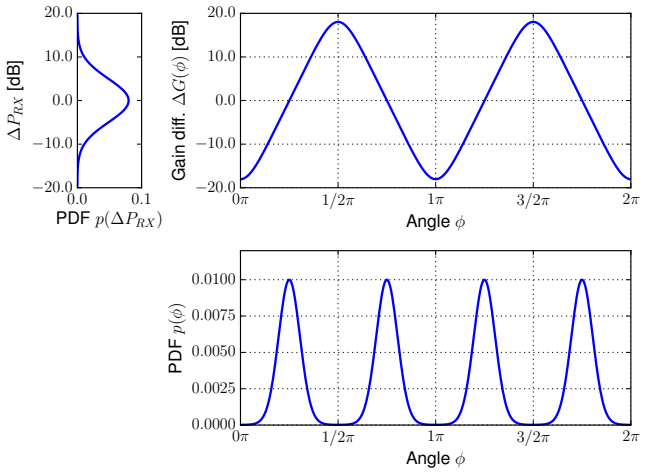

Figure 3: PDF for direction estimation: Exemplary measurement error distribution, gain difference function $\Delta G(\phi)$ and the DOA PDF $p(\phi)$ at $\sigma = 5\,\text{dB}$ and an observed RSSI difference of $\Delta P_{RX} = 0\,\text{dB}$.

II. Fundamentals of Field Strength-based Direction Finding

The DOA estimation is based on a field strength difference measurement of two directional antennas. In general, the received signal strength P_{RX} at a receiver from a transmitter can be calculated by:

$$P_{RX} = P_{TX} - L + G_{TX} + G_{RX}(\phi), \tag{1}$$

where P_{TX} is the emitted power of the transmitter, L is the path loss between transmitter and receiver, G_{TX} is the gain of the transmit antenna, and $G_{RX}(\phi)$ is the directional receive antenna gain as a function of the DOA ϕ of the electromagnetic wave (e.g. Figure 2). Using two identical antennas with different orientation, the antenna gain of the second antenna, e.g. $G_{RX,2}(\phi)$ can be described by the gain of the first antenna $G_{RX,1}(\phi)$:

$$G_{RX,1}(\phi) = G_{RX,2}(\phi - \nu), \tag{2}$$

where ν is the rotation angle between both antennas. With (2) the gain difference function ca be formulated as

$$\Delta G_\nu(\phi) = G_{RX}(\phi) - G_{RX}(\phi - \nu). \tag{3}$$

Then, the received signal strength difference ΔP_{RX} between both antennas is given by

$$\Delta P_{RX} = \Delta G_\nu(\phi), \tag{4}$$

when both channels are excited with same transmit power and exhibit exact the same path loss. The antenna gain patterns $G_{RX,1}(\phi)$ and $G_{RX,2}(\phi)$ are a priori known and therefore the pattern difference $\Delta G_\nu(\phi)$ is also known. Consequently, measuring the signal strength difference ΔP_{RX} between two differently orientated antennas the DOA φ can be calculated without knowledge of the path loss L, the transmit power P_{TX} and the transmit antenna gain G_{TX}.

In case of the BATS project, each of the antennas is described by two half-wave dipoles place uniformly on a circle with a radius of $r = 0.23\lambda$. The design process of antennas for RSSI-based direction finding has been described previously in [9] in a more general way. Considering the placement of dipoles described above the gain function for the directed antenna, according to [**?**], is expressed by

$$\text{G}(\phi) = 1.64 \cdot 2 \left[\cos(2\pi d \cos(\phi))\right]^2 , \tag{5}$$

which solely depends on the direction of arrival ϕ. The resulting gain patters for the antenna described above are depicted in Figure 2.

The gain difference function $\Delta G_\nu(\phi)$ for a set of two antennas is derived from (3) and (5), where ν is the rotation angle of the second antenna with respect to the first one implying that both antenna feature exactly the same gain pattern. In the BATS project a rotation angle $\nu = \frac{1}{2}\pi$ is considered, as this rotation angle yields the best average CRLB for the DOA estimation [9]. The resulting gain difference for the described antenna layout is shown in Figure 3.

It is obvious, that the given gain difference function results in an ambiguous DOA estimation result. Figure 3 depicts the transformation of gain difference function $\Delta G_\nu(\phi)$ (top right) with a standard deviation of $\sigma_{\Delta G} = 5\,\text{dB}$ for a measured RSSI difference of $0\,\text{dB}$ (top left). Evidently the DOA probability density function (PDF) has 4 modes (bottom) resulting from the symmetry of the contemplated gain patterns. These inherently arising ambiguities have to be resolved by multi-sensor data fusion. Therefore, the utilized fusion algorithms have to be able to handle multimodal distributions.

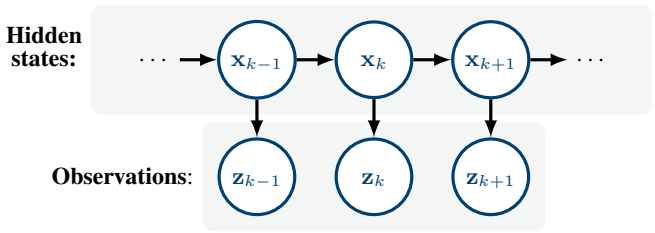

Figure 4: Observation of hidden states: The time-varying system is described by a first order hidden Markov Model (HMM).

III. Bayesian Filtering

In general, optimal filtering, more frequently known as Bayesian filtering, aims at the solution of estimating the hidden state of a time-varying system which is indirectly observed by measurements. Being the theoretic framework of the proposed grid-based filter in this section Bayesian filtering is reviewed. According to [14], the regarded state estimation problems are considered to have the following form

$$\begin{aligned} \mathbf{x}_k &\sim p(\mathbf{x}_k|\mathbf{x}_{k-1}) \\ \mathbf{z}_k &\sim p(\mathbf{z}_k|\mathbf{x}_k), \end{aligned} \tag{6}$$

where $\mathbf{x}_k$ is the hidden unknown state, that is observable by noisy measurements $\mathbf{z}_k$. Moreover, the distribution of the measurement likelihood $p(\mathbf{z}_k|\mathbf{x}_k)$ and the state transition PDF of the Markov process $p(\mathbf{x}_K|\mathbf{x}_{k-1})$ have to be known.

As shown in Figure 4 the observed time-varying system yields two essential properties:

1) Markov property of states [14]: The actual state $\mathbf{x}_k$ provided that $\mathbf{x}_{k-1}$ is independent of all previous states $(\mathbf{x}_0, \ldots, \mathbf{x}_{k-2})$ and the observation $\mathbf{z}_{1:k-1}$:
$$p(\mathbf{x}_k|\mathbf{x}_{1:k-1}, \mathbf{z}_{1:k-1}) = p(\mathbf{x}_k|\mathbf{x}_{k-1}) \tag{7}$$
2) Conditional independence of measurements [14]: The latest measurement $\mathbf{z}_k$ given the actual state $\mathbf{x}_k$ is independent of all previous measurements and the state history:
$$p(\mathbf{z}_k|\mathbf{x}_{1:k}, \mathbf{z}_{1:k-1}) = p(\mathbf{z}_k|\mathbf{x}_k) \tag{8}$$

When the desired state is $\mathbf{x}_k$, then the objective of Bayesian filtering is to represent the posterior PDF of a possible state representation comprising all measurements $p(\mathbf{x}_k|\mathbf{z}_{1:k})$. Applying Chapman-Kolmogorov equation for a posterior PDF $p(\mathbf{x}_{k-1}|\mathbf{z}_{1:k-1})$ given at time $k-1$ the prior PDF $p(\mathbf{x}_k|\mathbf{z}_{1:k-1})$ is derived by:

$$p(\mathbf{x}_k|\mathbf{z}_{1:k-1}) = \int p(\mathbf{x}_k|\mathbf{x}_{k-1}) p(\mathbf{x}_{k-1}|\mathbf{z}_{1:k-1}) d\mathbf{x}_{k-1}, \tag{9}$$

where $p(\mathbf{x}_k|\mathbf{x}_{k-1})$ is the PDF of the state transition. The successive posterior PDF is calculated in the update step applying the rule of Bayes to $p(\mathbf{x}_k|\mathbf{z}_k, \mathbf{z}_{1:k-1})$. Which then leads to the normalized product of the likelihood $p(\mathbf{z}_k|\mathbf{x}_k)$ and the PDF of the prior

$$p(\mathbf{x}_k|\mathbf{z}_{1:k}) = \frac{p(\mathbf{z}_k|\mathbf{x}_k) p(\mathbf{x}_k|\mathbf{z}_{1:k-1})}{p(\mathbf{z}_k|\mathbf{z}_{1:k-1})}. \tag{10}$$

As the denominator is constant relative to $\mathbf{x}_k$, it can be computed by integrating the nominator over $\mathbf{x}_k$. In summary, the posterior PDF can be calculated recursively applying prediction and update starting with an initial value for $p(\mathbf{x}_0|\mathbf{z}_0) = p(\mathbf{x}_0)$.

A. Grid-based Filter

In the BATS localization scenario a grid-based filter is utilized. In grid-based filters the total number of possible states is limited and the continuous state space is decomposed into so-called "cells" $\mathbf{x}_k^i : i = 1, \ldots, N$. Thus, its finite state space is defined by a grid of discrete states and also PDFs are discretized. The grid-based filter calculates the probability $p(\mathbf{x}_k|\mathbf{z}_{1:k})$ of the position $\mathbf{x}_k$ for every cell in the grid for the observed measurements $\mathbf{z}_{1:k}$. Under the assumption of a Markov properties (equations (11) and (12)) the position $\mathbf{x}_k$ at timestep k is described by:

$$\mathbf{x}_k = \mathbf{f}(\mathbf{x}_{k-1}) + \mathbf{w}_k \tag{11}$$
$$\mathbf{z}_k = \mathbf{g}(\mathbf{x}_k) + \mathbf{v}_k, \tag{12}$$

where $\mathbf{f}(\mathbf{x}_{k-1})$ describes the motion model of the system and $\mathbf{g}(\mathbf{x}_k)$ is the measurement model. $\mathbf{w}_k$ and $\mathbf{v}_k$ are process and measurement noise, respectively, and are mutually independent, with known PDFs.

The posterior PDF of the state x^i given the measurements $z_{1:k-1}$ is defined by

$$p(\mathbf{x}_{k-1} = \mathbf{x}^i|\mathbf{x}_{1:k-1}) = \omega_{k-1|k-1}^i \tag{13}$$

which can be written as a sum of delta functions

$$p(\mathbf{x}_{k-1}|\mathbf{x}_{1:k-1}) = \sum_{i=1}^{N} \omega_{k-1|k-1}^i \delta(\mathbf{x}_{k-1} - \mathbf{x}^i). \tag{14}$$

Recapitulating the Chapman-Kolmogorov equation (9) for the continuous case, the prior PDF for the discretized case becomes

$$\begin{aligned} p(\mathbf{x}_k|\mathbf{z}_{1:k-1}) &= \sum_{i=1}^{N} \sum_{j=1}^{N} \omega_{k-1|k-1}^j p(x^i|x^j) \delta(\mathbf{x}_{k-1} - \mathbf{x}^i) \\ &= \sum_{i=1}^{N} \omega_{k|k-1}^i \delta(\mathbf{x}_{k-1} - \mathbf{x}^i) \end{aligned} \tag{15}$$

where the new prior is weighted by a sum of delta functions and the new prior weights

$$\omega_{k|k-1}^i = \sum_{j=1}^{N} \omega_{k-1|k-1}^j p(\mathbf{x}^i|\mathbf{x}^j) \tag{16}$$

are calculated by reweighing the old posterior weights using the state transition probabilities. For the update step equation (10) becomes

$$p(\mathbf{x}_k|\mathbf{z}_{1:k}) = \sum_{i=1}^{N} \omega_{k|k}^i \delta(\mathbf{x}_{k-1} - \mathbf{x}^i), \tag{17}$$

where the posterior weights

$$\omega^i_{k|k} = \frac{\omega^i_{k|k-1} p(\mathbf{z}_k|\mathbf{x}^i)}{\sum_{j=1}^{N} \omega^j_{k|k-1} p(\mathbf{z}_k|\mathbf{x}^j)} \tag{18}$$

are the prior weights reweighed using the measurement likelihoods.

B. Forward-backward Smoothing

So far the grid-based filter only considered the measurements obtained before and at the current step for computing the best possible position estimate. However, for offline evaluations it is favored to estimate states for each timestep conditional on all the measurements that we have obtained. For offline processing the estimated trajectory can be smoothed applying Bayesian smoothing. In the grid-based filtering algorithm the cells probabilities $\omega^i_{k|k-1}$ are computed from the previous estimate applying the movement model

$$\omega^i_{k|k-1} = \sum_{j=1}^{N} \omega^j_{k-1|k-1} p(\mathbf{x}^i_k|\mathbf{x}^j_{k-1}). \tag{19}$$

Due to the Markov properties for a fixed interval this equation can be written in a reverse way, which then gives the backward prediction

$$\omega^i_{k|k+1} = \sum_{j=1}^{N} \omega^j_{k+1|k+1} p(\mathbf{x}^i_k|\mathbf{x}^j_{k+1}). \tag{20}$$

Combining the forward and backward filtering PDFs yields the smoothed localization estimate

$$\omega^i_{k|k} = \frac{\omega^i_{k|k-1} p(\mathbf{z}_k|\mathbf{x}^i_k) \omega^i_{k|k+1}}{\sum_{j=1}^{N} \omega^j_{k|k-1} p(\mathbf{z}_k|\mathbf{x}^j_k) \omega^j_{k|k+1}}. \tag{21}$$

IV. Grid-based Filter for Tracking Bats

After introducing the fundamentals of RSSI-based DOA estimation and reviewing the Bayesian filtering, in this section the realization of the grid-based filter is described in detail and the simulation environment is presented. In the first part the simulation environment is covered including trajectory generation, WSN, channel models and antenna characteristics. Secondly, the filter implementation comprising movement and measurement models.

A. Simulation Environment

The proposed filter algorithm is assessed in a simulation environment that incorporates multiple real-world effects of the localization system. Shadow fading effects are modeled by log-normal distributed fading. The organization of the simulation environment is depicted in Figure 5 and all blocks are described in detail in the following, where the grid-based filter and models of the localization block are covered in a separate Subsection IV-B due to their importance to this work.

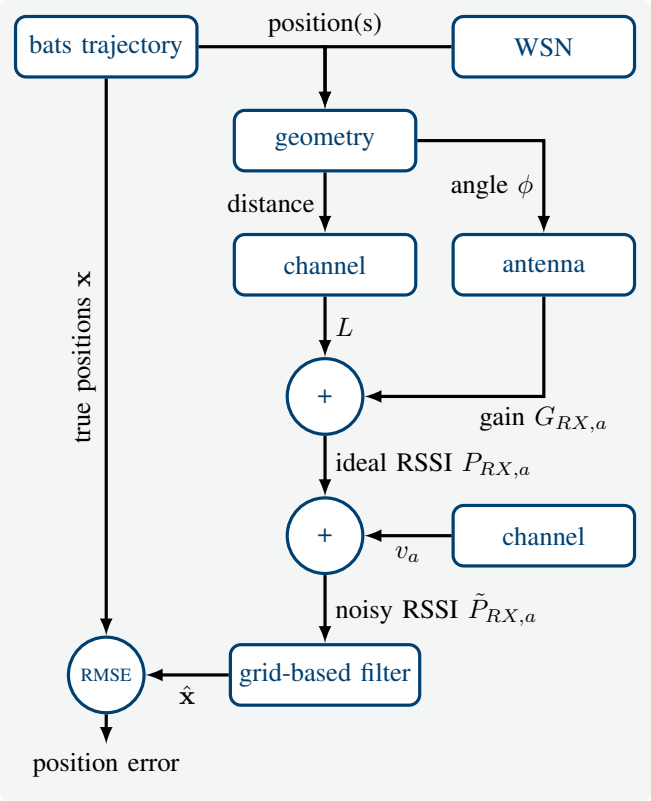

Figure 5: Block diagram of the simulation environment with the components for the geometrical dependencies, channel simulation and localization by the grid-based filter.

1) Trajectory Generation: Initially in the simulation environment, a bats trajectory is generated in the area of the base stations. In our case the trajectory is defined by 20 separate way points by the user and a linear interpolation at a defined speed is generating all 384 way points of the trajectory.

2) Topology of the Wireless Sensor Network: For the simulation the sensor nodes are placed in a shape shown in Figure 7, where the distance between the stations is roughly $50\,\mathrm{m}$ covering an area of $200\,\mathrm{m} \times 200\,\mathrm{m}$. The positions arrangement is defined like the positions of the stations in a field trail to make the results comparable in a later stage of the project. The main lobe direction of the antenna pattern $G_{RX,1}(\varphi)$ is rotated by $-15\,^\circ$ to the north direction and is indicated by the green arrows in Figure 7. The calculations for the optimal rotation angle to optimize the CRLB is shown in [**?**] and is not part of this paper. Considering the generated trajectory and the known positions of the base stations a, the distances r_a and angles ϕ_a between the way points and stations are calculated.

3) The Wireless Propagation Channel: The path loss L_{dB} is computed applying a modified version of the free space loss model and is defined by

$$L_{dB} = 17 + 10\log(r^{3,5}) + 20\log(f_c), \tag{22}$$

where r is the distance and f_c is the frequency. The underlying channel model was obtained during a measurement campaign

in the forests of the Franconia Switzerland close to Forchheim, Germany. The measurement frequency was in the short range devices band around $868\,\mathrm{MHz}$. All further simulations were carried out at a frequency of $868\,\mathrm{MHz}$. Details of utilized the channel sounding equipment has been recently published in [15].

4) Antenna Characteristics: The trajectory and the geometrical arrangement of the base stations defines the DOA ϕ_a of the received signal at every base station a, inherently, with this the antenna gain $G_{RX,1}(\phi_a)$ and $G_{RX,2}(\phi_a)$ is defined. The ideal RSSI values $P_{RX,a,1}$ and $P_{RX,a,2}$ are calculated with (1) for all positions of the trajectory along the given way points and for all receiving stations. For simplicity the index a is dropped in this section. The values are the ideal RSSI values $P_{RX,i}$ without any fading effects and would result to a perfect localization result. These artificial, error-free, measurements allow to test the localization algorithms and check whether the grid-based filter performs correctly, i.e. the estimator is free of biases. The generation of erroneous measurements, characterizing the impact of the wireless propagation channel, is specified in next paragraph.

5) Fading model: The true RSSI values $P_{RX,i}$ are superposed by correlated fading v_b and uncorrelated fading v_i

$$\tilde{P}_{RX,i} = P_{RX,i} + v_b + v_i \tag{23}$$

The shadow fading effect is modeled by log-normal fading [16], [17]. One effect considered is fading affecting both antennas in the same manner, i.e. correlated fading, defined by v_b. However, due to the evaluation of the field strength difference $\Delta P_{RX,a}$ this effect has no influence on the direction estimation.Although it does not lead to DOA estimation errors, the effect causes additional outages of stations due to the limited sensitivity of the receiver nodes as described in (29).

Furthermore, uncorrelated fading v_i is considered, adding additional noise to the measurements $\tilde{P}_{RX,1}$ and $\tilde{P}_{RX,2}$ individually. Due to the directional antenna pattern both antennas are sensitive to multipath propagation and shadowing, which is modeled by uncorrelated fading on both antennas, denoted by v_1 and v_2. For mutually independent v_1 and v_2 the measured RSSI difference becomes

$$\Delta\tilde{P}_{RX} = \Delta P_{RX} + v_1 - v_2 \tag{24}$$

The standard deviation of a sum of two uncorrelated noise processes $(v_1 - v_2)$ yields $\sqrt{2}\sigma_v$, when σ_v is defined as $\sigma_v = \sigma_{v_1}$ and $\sigma_{v_1} = \sigma_{v_2}$ is given. Therefore, the PDF of RSSI difference measurement is given by

$$p\left(\Delta\tilde{P}_{RX}\right) \propto \exp\left(-\frac{1}{2\sigma_v^2}\left[\Delta\tilde{P}_{RX} - \Delta P_{RX}\right]^2\right), \tag{25}$$

The noisy RSSI measurements $\Delta\tilde{P}_{RX,a}$ for all stations indexed by a are processed by the grid-based filter to estimate the position of the tracked target.

6) Position Estimation: The target position is estimated applying the grid-based filter. The grid size is determined with a cell spacing of $1\,\mathrm{m} \times 1\,\mathrm{m}$, which leads for a observation area of $200\,\mathrm{m} \times 200\,\mathrm{m}$ to a total number of 40000 cells. Simulations show that a cell size of $1\,\mathrm{m} \times 1\,\mathrm{m}$ is sufficient to obtain accurate position estimates. In addition, this grid size still yields an acceptable computational load.

The localization comprises three modes: i.e. position estimates from pure snapshot measurements, filter estimates applying the grid-based filter and the latter including forward-backward smoothing. The localization results are discussed in Section V.

B. Bayesian Filter Models

In this section the filter models of the proposed grid-based filter are discussed. The grid-based filter incorporates a motion model (11) of the bat to predict the state for the successive timestep and a measurement model (12) based on the PDF for RSSI-based DOA estimation described by (25).

1) Motion Model : State prediction is a essential part of Bayesian filters. A priori knowledge of the movement model of the tracked target is beneficial. However, the flight behavior of many animals and insects is typically characterized by Levy flights as shown in [18] and [19]. According to observations of the biologists, the flight behavior of bats seems to be rather random, and thus is very similar to Levy flights. For the sake of simplicity the movements are modeled by a motion of the target in an arbitrary direction with a limited speed, independent of the movement in the previous timestep, which is expressed by

$$\mathbf{x}_k = \mathbf{x}_{k-1} + \exp(-j\varphi) \cdot \Delta x_{move}, \tag{26}$$

where $\mathbf{x}_k$ is the predicted position, the previous $\mathbf{x}_{k-1}$, and φ and Δx_{move} are sampled form uniform distributions defined by$\varphi \sim \mathcal{U}(-\pi, \pi)$ and $\Delta x_{move} \sim \mathcal{U}(0, \Delta_x max)$The maximum speed is limited to the physical maximum possible speed of a bat v_{max} . The maximum possible movement in state transition is therefore denoted by

$$\Delta x_{max} = v_{max} \cdot (t_k - t_{k-1}), \tag{27}$$

where $t_k - t_{k-1}$ is the time between two measurements.

The PDF for the cell transition probability $p(\mathbf{x}^i|\mathbf{x}^j)$ is defined as

$$p(\mathbf{x}^i|\mathbf{x}^j) \propto \begin{cases} 1 & ||\mathbf{x}^i - \mathbf{x}^j||_2 \leq \Delta x_{max} \\ 0 & \text{otherwise} \end{cases}. \tag{28}$$

The new prior weight is computed following equation (16). The full discrete prior PDF of the grid-based filter is calculated according to equation (15).

2) Measurement model: The measurement model of the grid-based filter realizes the update base upon the RSSI difference measurements incorporating the model presented in Section II. For the simulated noisy measurements values $\tilde{P}_{RX,a,i}$ of station a the RSSI difference $\Delta\tilde{P}_{RX,a}$ is evaluated when both RSSI values fulfill

$$P_{min} < \tilde{P}_{RX,a,i} < P_{max}, \tag{29}$$

where P_{min} is the minimum received signal strength e.g. the sensitivity of the receiver, and P_{max} is the maximum received signal strength, e.g. clipping of the receiver.

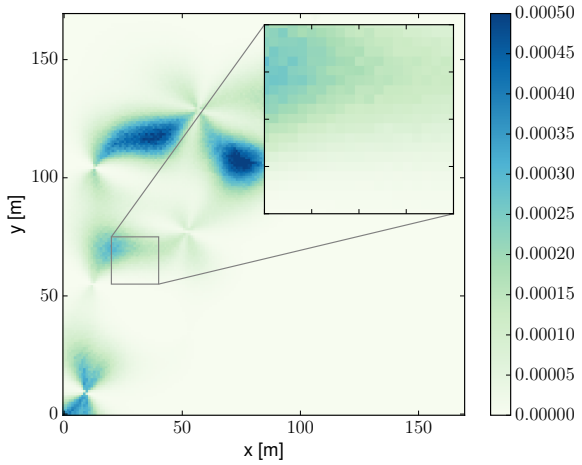

(a) Measurement PDF snapshot.

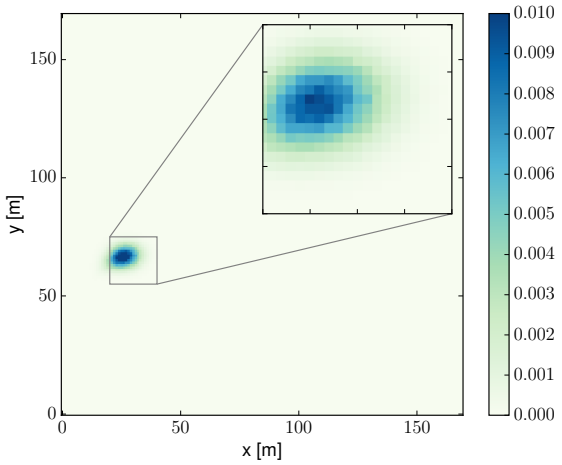

(b) Grid-based filter PDF snapshot.

Figure 6: Discrete PDF snapshots for (a) position probability from snapshot measurement and (b) position probability after update step of the grid-based filter are depicted above.

Now, the measurement model $g_a(\mathbf{x})$ for single receiver station a for the state vector $\mathbf{x} = [x, y]^T$ is defined as

$$g_a(\mathbf{x}) = \Delta G_a \left(\tan^{-1} \frac{\Delta y_a}{\Delta x_a} \right), \tag{30}$$

with

$$\Delta x_a = x - x_a \quad and \quad \Delta y_a = y - y_a. \tag{31}$$

When further defining the measured RSSI difference for station a as

$$z_a = \Delta \tilde{P}_{RX,a}, \tag{32}$$

the measurement probability $p(z_{k,a}|\mathbf{x}_k)$ for station a and a measurement $z_{k,a}$ given the state $\mathbf{x}_k$ expressed by

$$p(z_{k,a}|\mathbf{x}_k) \propto \exp\left(-\frac{1}{2\sigma_v^2} \left[z_{k,a} - g_a(\mathbf{x}_k) \right]^2 \right) \tag{33}$$

where the PDF is normal distributed as the fading model is log-normal fading and RSSI is measured in dB and $g_a(\mathbf{x}_k)$ yields the expected field strength difference for the given state vector and σ_v^2 is the expected measurement noise variance. Applying (33) and assuming all measurement to be independent, the probability $p(\mathbf{z}_k|\mathbf{x}_k)$ for the measured field strength differences $\mathbf{z}_k$ is calculated by multiplying the measurement likelihoods for all the contributing receivers

$$p(\mathbf{z}_k|\mathbf{x}_k) \propto \prod_{a=1}^{A} p(\mathbf{z}_{k,a}|\mathbf{x}_k), \tag{34}$$

where A is the number of stations and

$$\mathbf{z}_k = [z_{k,1}, z_{k,2}, \ldots, z_{k,A}]^T. \tag{35}$$

Finally, the weights $\omega_{k|k}^i$ of the respective cell i representing the state $\mathbf{x}_k^i$ are calculated according to

$$\omega_{k|k}^i \propto \omega_{k|k-1}^i \cdot p(\mathbf{z}_k|\mathbf{x}_k^i), \tag{36}$$

with $\omega_{k|k-1}^i$ being the predicted weight for cell i. The posterior PDF is computed applying equation (17). The most probable position estimate is extracted from the discrete PDF utilizing the k-nearest neighbors algorithm.

V. Simulations Results

As stated before, the measurement PDF is highly multimodal. The impact of this multimodality is visualized in Figure 6a. The position probability given a snapshot measurement $p(\mathbf{x_k}|\mathbf{z}_k)$ is depicted. A large number of position hypotheses arises from a single measurement. Moreover, Figure 6a illustrates that the largest weights of the measurement PDF are not even in the vicinity of the true mean. However, in contrast to the position calculation using a measurement snapshot, the grid-based filter PDF shows a decent Gaussian-like distribution centered around the true mean. Note that the PDFs in Figure 6a have different scales.

The computed positions for the snapshot measurements, filtered and smoothed estimates are compared to the true mean. The simulation run has a length of 384 steps. Correlated fading effects were simulated using $\sigma_{v_b} = 10\,\mathrm{dB}$. Three different uncorrelated fading effects were simulated using $\sigma_{v_i} = \{2\,\mathrm{dB}, 5\,\mathrm{dB}, 10\,\mathrm{dB}\}$. In Figure 7 the true trajectory is shown as a red line, the localized path of the forward-backward smoothed trajectory is shown as a blue line for different fading levels. The higher the level of fading is, the more diverges the estimated path from the true trajectory. The root-mean-square error (RMSE) for the forward-only grid-based filter and for the forward-backward smoothing filter shown in Table I. As expected, increasing the measurement noise the

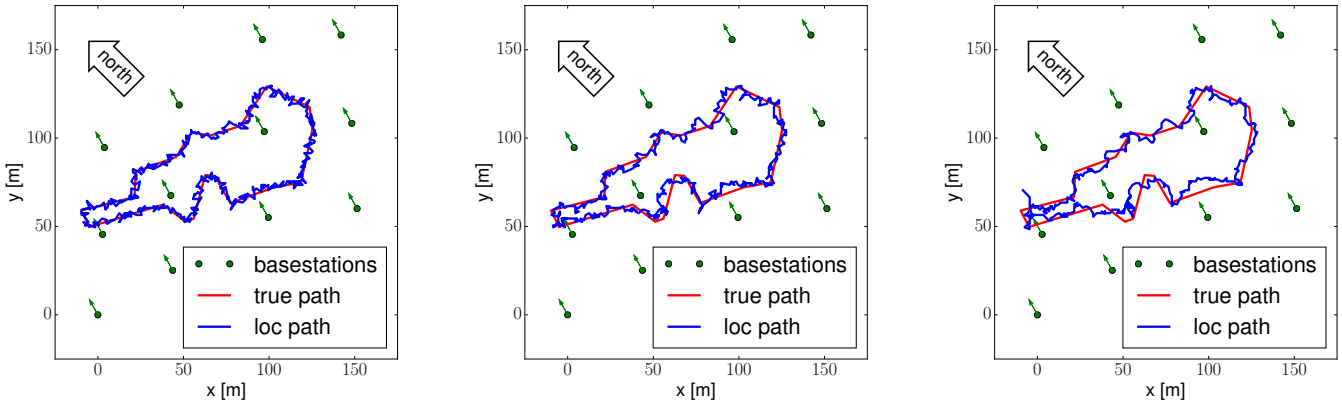

(a) $\sigma_{zi} = 2\,\mathrm{dB}$ (b) $\sigma_{zi} = 5\,\mathrm{dB}$ (c) $\sigma_{zi} = 10\,\mathrm{dB}$

Figure 7: Reference trajectory (red line), the estimated trajectory of grid-based filter (blue line) and sensors nodes (green dots). Fading levels of $\sigma_{zb} = 10\,\mathrm{dB}$ and $\sigma_{zi} = \{2\,\mathrm{dB}, 5\,\mathrm{dB}, 10\,\mathrm{dB}\}$

error in the position estimate increases. The use of the grid-based filter with forward-backward smoothing reduces position error significantly, compared with using the grid-based filtering without smoothing. Resulting errors for both filter variants over the simulated path are shown in Figure 8 for $\sigma_{v_b} = 10\,\mathrm{dB}$. On can see, that filtering and smoothing significantly reduces the RMSE, in particular the smoothed filter error stay well below $10\,\mathrm{m}$ for the whole trajectory, whereas the mean error of the snapshot positioning substantially exceeds this value.

For the targeted application, wildlife tracking, the errors are in a acceptable range and bats movement pattern can be tracked. The processing load is rather high due to the high number of cells. The cell density is uniform over the covered area of observation, also in areas with low residence probability of the bats. The forward-backward smoothing enables a robust localization, even for the initial phase of the location tracking. A simple forward filtering algorithm might fail in this phase due to the highly multimodal distribution. Tracking the wrong starting point takes the filter a long time to recover and track the true hypothesis, which then will lead to large position estimation errors.

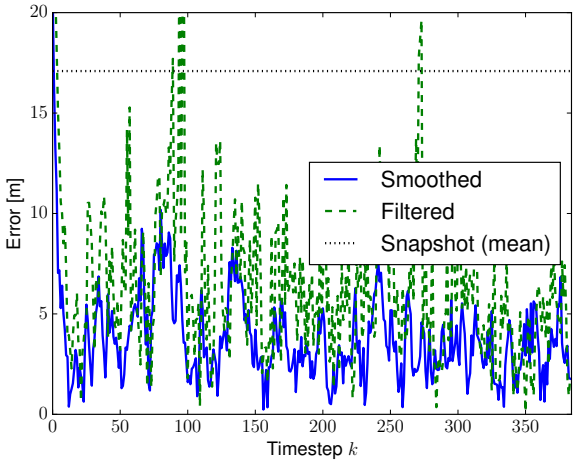

Figure 8: localization errors by way points for a forward filter implementation and a forward-backward smoothing filter implementation

VI. Conclusion

The proposed grid-based filter shows the ability to handle multimodal distributions arising from a ambiguous DOA estimation based on RSSI measurements. The localization performance even in presence of massive fading is remarkable.

Filter type	**Noise** (σ_{zi})		
	2 dB	5 dB	10 dB
Snapshot positioning	2.60 m	6.54 m	17.09 m
Forward-only filter	2.41 m	3.99 m	6.48 m
Forward-backward filter	1.94 m	2.65 m	3.76 m

Table I: RMSE for grid-based filter.

One major drawback of the grid-based filter is the high computational load, it scales linear to area of observation and cell size, therefore, it scales badly to enlarging the observation area. Furthermore, the density of cells is fixed even in areas with low spatial probability of a bat. Simulations showed a cell size of $1\,\mathrm{m}$ by $1\,\mathrm{m}$ is sufficient up to a localization accuracy of $1.5\,\mathrm{m}$.

For further investigation a particle filter should be addressed. Scaling down the number of particles lowers the computational load. However, this approach, most likely, will bring up new challenges, e.g. particle depletion. Future work will include results from field trials in the Franconian forests and will be compared to the simulation results presented in this paper.

Furthermore, sub-optimal Bayesian filter algorithms and more sophisticated channel model are a subject a further research.

ACKNOWLEDGMENT

This work is funded by the German Science Foundation DFG grant FOR 1508, Research Unit BATS.

REFERENCES

[1] Alan Mainwaring, David Culler, Joseph Polastre, Robert Szewczyk, and John Anderson. Wireless sensor networks for habitat monitoring. In *Proceedings of the 1st ACM international workshop on Wireless sensor networks and applications*, pages 88–97. ACM, 2002.

[2] Antonio-Javier Garcia-Sanchez, Felipe Garcia-Sanchez, Fernando Losilla, Pawel Kulakowski, Joan Garcia-Haro, Alejandro Rodriguez, Jose-Vicente Lopez-Bao, and Francisco Palomares. Wireless Sensor Network Deployment for Monitoring Wildlife Passages. *Sensors*, 10(8):7236–7262, 2010.

[3] Bernd-Ulrich Rudolph, Alois Liegl, and Otto Von Helversen. Habitat selection and activity patterns in the greater mouse-eared bat myotis myotis. *Acta Chiropterologica*, 11(2):351–361, 2009.

[4] R Arlettaz. Feeding behaviour and foraging strategy of free-living mouse-eared bats, myotis myotisandmyotis blythii. *Animal behaviour*, 51(1):1–11, 1996.

[5] Simon P Ripperger, Elisabeth KV Kalko, Bernal Rodríguez-Herrera, Frieder Mayer, and Marco Tschapka. Frugivorous bats maintain functional habitat connectivity in agricultural landscapes but rely strongly on natural forest fragments. *PloS one*, 10(4), 2015.

[6] Craig S Smith, Jonathan H Epstein, Andrew C Breed, Raina K Plowright, Kevin J Olival, Carol de Jong, Peter Daszak, and Hume E Field. Satellite telemetry and long-range bat movements. *PloS one*, 6(2), 2011.

[7] Thomas Kunz. Radiotelemetry: Techniques and analysis. In *Ecological and behavioral methods for the study of bats*, pages 57–77. Johns Hopkins University Press, Baltimore, Baltimore, 2009.

[8] Martin Hierold, Simon Ripperger, Darija Josic, Frieder Mayer, Robert Weigel, and Alexander Koelpin. Low-weight wireless sensor network for encounter detection of bats. In *IEEE Topical Conference on Wireless Sensors and Sensor Networks*, 2015.

[9] Markus Hartmann, Oliver Pfadenhauer, Lucila Patino-Studencka, Hans-Martin Tröger, Albert Heuberger, and Jörn Thielecke. Antenna pattern optimization for a rssi-based direction-of-arrival localization system. In *ION's Pacific PNT Conference 2015*, pages 429–433, Honolulu, Hawaii, April 2015.

[10] Markus Hartmann, Thorsten Nowak, Jörg Robert, Hans-Martin Tröger, Albert Heuberger, and Jörn Thielecke. A low-cost rssi based localization system design for wildlife tracking. In *Radio and Antenna Days of the Indian Ocean 2015*, 2015.

[11] B.R.S. Arulampalam. *Beyond the Kalman Filter: Particle Filters for Tracking Applications*. Artech House, 2004.

[12] Sebastian Thrun, Wolfram Burgard, and Dieter Fox. *Probabilistic robotics*. MIT press, 2005.

[13] M.S. Arulampalam, S. Maskell, N. Gordon, and T. Clapp. A tutorial on particle filters for online nonlinear/non-gaussian bayesian tracking. *Signal Processing, IEEE Transactions on*, 50(2):174–188, Feb 2002.

[14] Simo Särkkä. *Bayesian Filtering and Smoothing*. Cambridge University Press, 2013.

[15] H. Lieske, T. Lauterbach, J. Robert, G. Kilian, and A. Heuberger. Indoor-to-Outdoor Radio Channel Measurements in sub-GHz Unlicensed Frequency Bands. In *Smart Objects, Systems and Technologies (SmartSysTech), Proceedings of 2015 European Conference on*, Aachen, June 2015.

[16] D.C. Cox, R.R. Murray, and A.W. Norris. 800-MHz attenuation measured in and around suburban houses. *AT&T Bell Laboratories Technical Journal*, 63(6):921–954, 1984.

[17] John S. Seybold. *Introduction to RF propagation*. John Wiley & Sons, 2005.

[18] CliffordT. Brown, LarryS. Liebovitch, and Rachel Glendon. Lévy flights in dobe ju/'hoansi foraging patterns. *Human Ecology*, 35(1):129–138, 2007.

[19] Andy M. Reynolds and Mark A. Frye. Free-flight odor tracking in drosophila is consistent with an optimal intermittent scale-free search. *PLoS ONE*, 2(4):e354, 04 2007.